PERGAMON

International Journal of Multiphase Flow 26 (2000) 999–1018

International Journal of Multiphase Flow

www.elsevier.com/locate/ijmulflow

The effects of geometry, fluid properties and pressure on the hydrodynamics of gas–liquid cylindrical cyclone separators

S. Movafaghian[a], J.A Jaua-Marturet[a], R.S. Mohan[a], O. Shoham[a,*], G.E. Kouba[b]

[a]*The University of Tulsa, 600 S College Avenue,Tulsa, OK 74104, USA*
[b]*Chevron Petroleum Technology Company, 2811 Hayes Road, Houston, TX 77082, USA*

Received 24 October 1998; received in revised form 23 June 1999

Dedicated to the memory of Juan Andres Jaua-Marturet who passed away during the course of this investigation.

Abstract

The hydrodynamic flow behavior in a Gas–Liquid Cylindrical Cyclone (GLCC) compact separator is studied experimentally and theoretically. New experimental data are acquired utilizing a 7.62 cm I.D, 2.18 m high, GLCC separator for a wide range of operating conditions. Investigated parameters include three different inlet geometries (5.08 cm I.D single, 7.62 cm I.D single and 7.62 cm I.D dual inlets), four different liquid viscosities (1, 2.5, 5 and 10 cps), three system pressures (101.3, 273.6 and 487.2 kPa), and the effect of surfactant. The measured data comprise of equilibrium liquid level, zero-net liquid flow holdup and the operational envelope for liquid carry-over. The data are utilized to verify and refine an existing GLCC mechanistic model. Comparison between the modified model predictions and the experimental data show a very good agreement.

Keywords: Gas–liquid cylindrical cyclone; GLCC geometry; Separation; Flow-hydrodynamics; Liquid carry-over; Fluid properties

* Corresponding author. Petroleum Engineering Department, The University of Tulsa, Tulsa, OK 74104, USA. Tel.: +1-918-631-3255; fax: +1-628-631-2059.

E-mail address: os@utulsa.edu (O. Shoham).

0301-9322/00/$ - see front matter
PII: S0301-9322(99)00076-2

1. Introduction

For the past several decades conventional, gravity based, vessel-type separators, that are bulky and expensive, have been extensively used in the field. In recent years, due to economical and operational pressures, the industry has shown keen interest in the development and application of alternatives to the conventional separators, in the form of compact separators. One such alternative is the Gas–Liquid Cylindrical Cyclone (GLCC), which is a simple, compact, low weight, low-cost separator, that requires minor maintenance and is easy to install and operate.

The GLCC, shown schematically in Fig. 1, is simply a vertically installed pipe section, mounted with a downward inclined tangential inlet, with two outlets provided at the top and the bottom. It has neither moving parts nor internal devices. The tangential inlet provides a swirling motion and the gas and liquid phases are separated due to the centrifugal and gravitational forces. The liquid is forced towards the cylinder's wall and exits at the bottom, while the gas moves to the center of the cyclone and leaves at the top.

The GLCC has a wide range of potential applications, varying from partial separation to a complete phase separation (Bandyopadhyay et al., 1994; Nebrensky et al., 1980; Zhikarev et al., 1985). Potential applications include: control of gas/liquid ratio for multiphase flow meters, pumps (Arato and Barnes, 1992), and de-sanders; portable well test metering; flare gas scrubbing; primary separation; and pre-separation upstream of slug-catchers or primary separators. Successful GLCC field applications have demonstrated the pronounced impact that this technology is bound to have on the industry. However, scarcity of experimental data and models, and lack of understanding of hydrodynamic flow behavior in the GLCC prevent complete confidence in its design and necessitates additional research and development. Knowledge of the flow behavior in the GLCC will enable the development of more accurate design tools to make the GLCC an attractive alternative to the conventional separator.

As it is an emerging technology, very little literature is available on the optimum design and performance of GLCCs. A brief review of the references dealing with the industrial

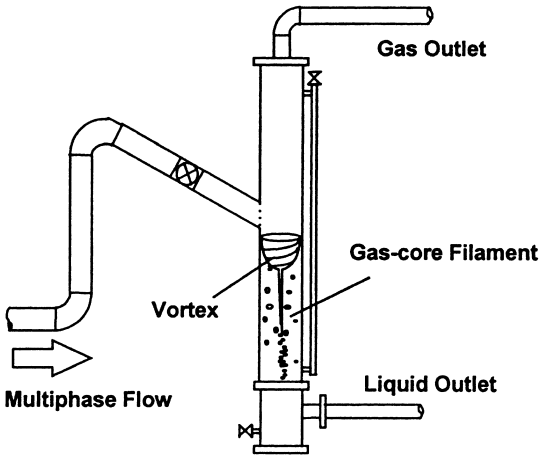

Fig. 1. Schematic of GLCC separator

applications, experimental investigations, mechanistic modeling and computational fluid dynamics (CFD) simulations of GLCC is given below.

Despite the difficulty to predict the performance of the GLCC, it has been used for sub-sea separation and pumping facilities (Baker and Entress, 1992), and geothermal applications for both down-hole and surface separation (Kanyua and Freeston, 1985). Cyclones and similar equipment have also been used for a better handling of slug flow in offshore platforms (Cowie, 1991; Oranje, 1990; Davies and Watson, 1979) and natural gas transmission systems (Forsyth, 1984). Weingarten et al. (1995) have developed a cylindrical cyclone with spiral vane internals, namely, the Auger separator, and explored the utilization of a liquid level passive control system.

Recently, the GLCC has been used as part of a multiphase flow metering loop. In this configuration, the gas and liquid phases are separated in the GLCC. Each of the separated phases is metered by a single-phase flow meter installed in the respective outlets of the GLCC. The gas and liquid legs are recombined downstream of the meters to form two-phase flow. As reported by Kouba et al. (1995) and Kouba and Shoham (1996), the GLCC metering loop is gaining popularity in the industry, with over 100 field applications in operation. It utilizes proven, of-the-shelf, single-phase metering technology, and saves significant amount of money, avoiding the utilization of full bore multiphase flow meters, which are still in the developmental stage.

Experimental and theoretical studies on the detailed hydrodynamic flow behavior in the GLCC are scarce. Millington and Thew (1987) reported local tangential and axial velocity distribution measurements in a cyclone separator. Reydon and Gauvin (1981) studied the behavior of confined vortex flow in conical cyclones. Through a study of gas–liquid flow in a spiral horizontal cyclone with vortex generator, Kurokawa and Ohtaik (1995) confirmed the existence of a complex velocity profile. An efficiency computation based on the analysis of the droplet trajectories in liquid–liquid hydrocyclones was presented by Wolbert et al. (1995). The study of Kouba et al. (1995) and Kouba and Shoham (1996) presents the first experimental results for air–water system and the effect of inlet inclination angle, operating pressure, body and inlet geometry on liquid carry-over phenomenon for single-stage and multi-stage GLCCs. This study also presents an initial foundation of a mechanistic model for the GLCC separator.

Experimental data of GLCC operational envelope and a mechanistic model for GLCC separators have been reported by Arpandi et al. (1996). The developed model enables the prediction of the operational envelope for liquid carry-over. Marti et al. (1996) presented an analysis of bubble trajectory by applying a force balance on an individual bubble. Simulation of the flow behavior in GLCC separator applying a Computational Fluid Dynamics (CFD) approach was presented for single-phase and two-phase flow by Erdal (1996) and Erdal et al. (1996). Recently, Motta et al. (1997) presented a simplified CFD model for rotational two-phase flow in a GLCC separator. The model assumes an axisymmetric flow and three velocity components, applicable to steady-state and isothermal conditions.

Above literature review reveals that more studies need to be conducted in order to make the GLCC a more predictable, reliable and viable tool for the industry. The goal of the current study is to investigate and shed more light on the hydrodynamic flow behavior in the GLCC. The specific objectives of the study are to acquire, for the first time, data on the hydrodynamic flow in the GLCC, focusing on the effect of fluid properties, GLCC geometry, and pressure.

The data are used to validate and refine the GLCC mechanistic model developed previously by Arpandi et al. (1996).

2. Experimental program

2.1. Test facility

The experimental two-phase flow-loop is comprised of a standard metering section for measurement of the gas and liquid flow rates, and a GLCC test section where the experimental data are acquired. Details of the metering section are given in Movafaghian (1997). Following is a brief description of the test facility.

2.1.1. Test section

The test section is comprised of a GLCC separator, configured in a multiphase flow metering loop, as shown in Fig. 2. The GLCC metering loop consists of the GLCC body, an inclined inlet, a gas leg with a gas vortex shedding meter, a liquid leg with a liquid mass flow meter, and a recombination section, all manufactured from transparent PVC R-4000 pipe.

The two-phase mixture is introduced into the GLCC through a 1.14 m long, -27° inclined inlet. The flow enters the GLCC body, passing through a slot having an area of 25% of the inlet cross sectional area. Two inlet configurations are used, namely, 5.08 and 7.62 cm I.D. The inlet can be operated as dual-inlet (both valves on the upper and lower sections are open) or as

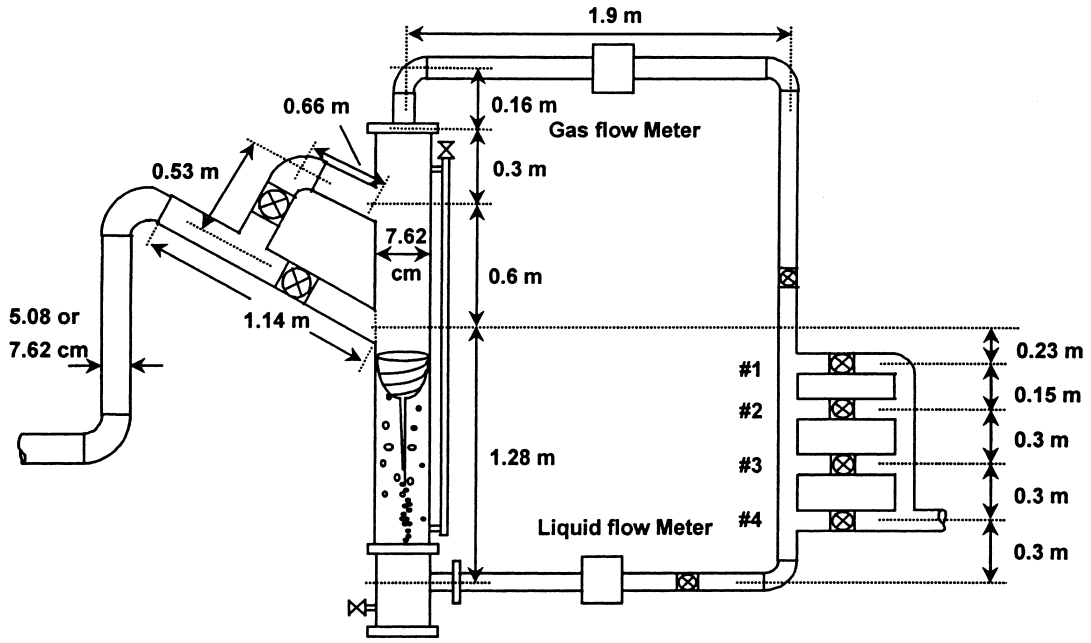

Fig. 2. GLCC test section schematic.

a single-inlet (upper-inlet valve closed and lower-inlet valve open, as shown in Fig. 2). In the dual-inlet configuration, the upper inlet (0.66 m long) receives mainly gas, providing a pre-separation of the phases and, thus, a better overall separation efficiency for the GLCC.

The GLCC body is 7.62 cm I.D and 2.18 m high. The lower-inlet is located 1.28 m from the bottom and 0.9 m from the top of the GLCC. The liquid and gas legs are 1.9 m long. The gas and liquid legs and the recombination sections are made of 5.08 cm I.D. pipe. Several recombination points are available, designated as #1, #2, #3 and #4, as shown in Fig. 2. The first recombination point is located 0.23 m below the lower-inlet plane.

2.1.2. Instrumentation and data acquisition system

The GLCC is equipped with a level indicator (sight gauge) installed parallel to the body of the separator. The separated gas and liquid phases are metered by means of a gas vortex shedding meter (located on the gas leg) and a Micromotion® mass flow meter (on the liquid leg). The pressure is measured by two transducers located upstream and downstream of the GLCC. The temperature and density of the liquid phase are also measured by the Micromotion® mass flow meter.

All the 15 output signals from the sensors, transducers, and metering devices are acquired using a computer based data acquisition system. The sampling rate was set at 2 Hz for a 2 min sampling period. The final measured quantity results from an arithmetic averaging of 240 readings, when steady-state condition is established.

2.2. Physical phenomena

This section contains discussion and definitions of the fundamental two-phase flow phenomena occurring in the GLCC. The discussion will enable a better understanding of the experimental results, which will be presented next.

2.2.1. Liquid carry-over and gas carry-under

Efficient operation of the GLCC is limited by two undesirable phenomena, namely, liquid carry-over and gas carry-under. An a priori knowledge of these limiting boundaries is needed for proper design and operation of the GLCC.

Liquid carry-over refers to the entrainment of liquid into the discharged gas stream at the top of the GLCC. It occurs under extreme operating conditions of high gas and/or high liquid flow rates. The locus of the superficial liquid velocity versus the superficial gas velocity in the GLCC, at which liquid carry-over is initiated, provides the operational envelope for liquid-carry over. For flow conditions below the envelope, no liquid carry-over occurs. The region above the operational envelope represents the conditions for which continuous liquid carry-over occurs.

Entrainment of gas into the exiting liquid stream from the GLCC bottom is referred to as gas carry-under. Below the vortex, relatively large gas bubbles move radially inward and form the gas-core-filament (see Fig. 1). Three mechanisms have been identified as possible ways by which gas is carried-under with the liquid phase. These are: presence of shallow radial trajectory of small individual bubbles preventing from coalescing with the gas-core-filament; gas-core-filament instability, which results in the gas-core-filament whipping helically and

occasionally breaking off, producing small bubbles that might be carried-under; and, a bubble swarm instability, which occurs with a sudden increase of the liquid flow rate, producing a cloud of the bubbles that are unable to migrate to the gas-core-filament.

2.2.2. Equilibrium liquid level

The distribution of the gas–liquid interface within the cyclone is very complex due to churning and fluctuating behavior of the flow in the GLCC. Therefore, it is necessary to consider the equilibrium liquid level. This is the liquid level that is measured using the liquid level indicator (sight gauge). In a closed-loop configuration, the equilibrium liquid level is determined by a pressure balance from the inlet to the point of recombination, between the gas leg and the liquid leg across the GLCC.

2.2.3. Zero-net liquid flow holdup

The zero-net liquid flow holdup, for a given gas flow rate, is the maximum liquid holdup that the GLCC can tolerate in its upper part above the inlet, prior to initiation of liquid carry-over. Under these conditions, although two-phase flow is observed in the upper part of GLCC, only gas is produced from the top, while the liquid phase churns up and down, providing a zero-net liquid flow. Knowledge of the liquid holdup prior to liquid carry-over is crucial for a better understanding of the liquid carry-over phenomenon.

2.3. Experimental results

This section presents, for the first time, experimental results on the effect of GLCC geometry, fluid physical properties and pressure on the hydrodynamic flow behavior in the GLCC.

2.3.1. Effect of inlet geometry

Fig. 3 illustrates the variations of the operational envelope for liquid carry-over with the GLCC inlet configuration, at atmospheric pressure for an air–water system. For all the cases presented, the GLCC body is the same, namely, 7.62 cm I.D, and the only difference is the inlet diameter and configuration. Three different inlet configurations were used: a 5.08 cm I.D single-inlet, a 7.62 cm I.D single-inlet and a 7.62 cm I.D dual-inlet.

Comparison between the liquid carry-over operational envelopes for the 5.08-cm and the 7.62-cm I.D single-inlet GLCCs reveals that operational envelope expands marginally for the 7.62-cm inlet due to a better pre-separation at the inlet section. The most interesting results are shown for the dual-inlet configuration. The dual-inlet configuration is much superior to the single-inlet for superficial gas velocities below 7 m/s. For higher superficial velocities, above 7 m/s, the performance of the single-inlet GLCC is better than that of the dual-inlet. This is due to a change in the flow pattern from slug flow (lower superficial gas velocities) to annular flow (higher superficial gas velocities), upstream of the GLCC. The inclined inlet causes stratification to occur in the lower inlet, and gas flows primarily through the upper inlet, increasing the extent of the operational envelope for liquid carry-over. However, for high gas flow rates, under annular flow, liquid is carried into the upper inlet causing earlier liquid carry-

over from the GLCC. The liquid carry-over under these conditions is dependent upon the distance between the upper inlet and the gas outlet of the GLCC.

The performance of the dual-inlet configuration is superior to the single-inlet configuration only for conditions approaching the operational envelope for liquid carry-over. Equilibrium liquid level data taken for both the 7.62-cm I.D single and dual inlet GLCCs for flow conditions below the operational envelope, where no liquid carry-over is encountered revealed that, for these conditions the results for the single-inlet and dual-inlet configurations are similar.

2.3.2. *Effect of recombination point*

The three recombination locations are determined by valves numbered 1, 2 and 3, located at distances 0.23, 0.38 and 0.68 m below the inlet plane, respectively (see Fig. 2). The effect of the recombination location on the operational envelope for liquid carry-over is shown in Fig. 4 for the 5.08-cm I.D single-inlet GLCC. As can be seen, lowering the recombination point expands the operational envelope for liquid carry-over. However, one must realize that as the recombination point is lowered, the equilibrium liquid level in the GLCC reduces, which may result in undesirable gas carry-under. Convergence of the three envelopes is observed at a superficial gas velocity of approximately 11.5 m/s. This is the gas velocity at which transition to fully annular flow is encountered at the GLCC inlet.

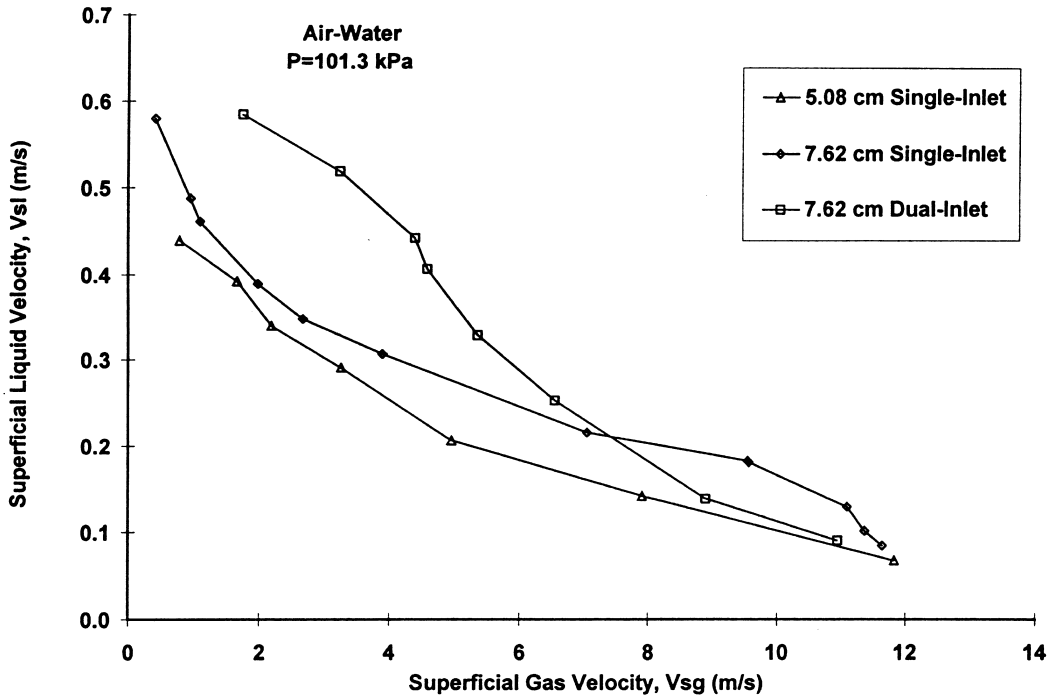

Fig. 3. Effect of inlet geometry on operational envelope for liquid carry-over.

2.3.3. Effect of fluid properties

Several tests have been carried out with various liquid viscosities and with foam generating surfactant. The viscosifier additive used is FlowPaam® 3530S polymer (a partially hydrolyzed polyacrylamide), while the surfactant additive is Tergitol® Min-Foam 2X (a mixture of 11–15 carbon, linear secondary alcohol with ethylene oxide and propylene oxide). The fluid properties were monitored continuously during the experimental test runs.

2.3.3.1. Effect of viscosity. The effect of increase in viscosity is to increase the equilibrium liquid level in the GLCC. This is due to the increase in frictional losses in the liquid leg, which in turn causes higher liquid levels in the GLCC. Fig. 5 shows a comparison of the equilibrium liquid level for four liquid viscosities of 1, 2.5, 5, and 10 cps, for a fixed superficial gas velocity of 1.52 m/s. As can be seen, the liquid level "shifts" upward for higher viscosities. A similar trend was obtained for superficial gas velocities of 4.57 and 6.10 m/s (Movafaghian, 1997).

Examination of operational envelope for liquid carry-over for the 1, 2.5, 5 and 10 cps cases reveals a continuous reduction of the operational envelope with increase in liquid viscosity, as shown in Fig. 6. This is consistent with the hydrodynamics of the flow. The increase in equilibrium liquid level, as the viscosity increases, causes earlier liquid carry-over at lower gas and liquid flow rates.

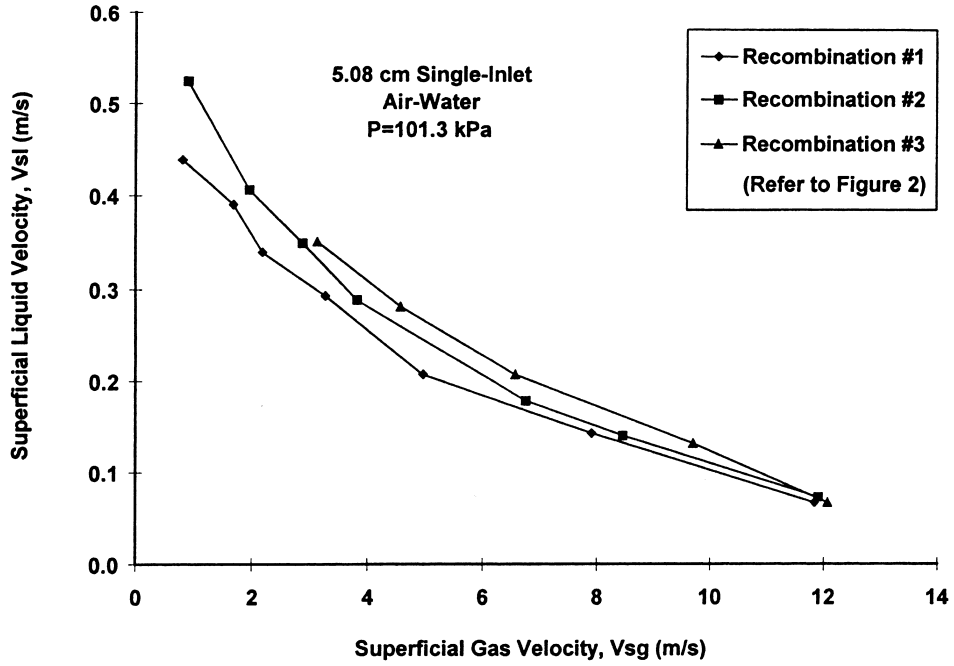

Fig. 4. Effect of recombination point on operational envelope for liquid carry-over.

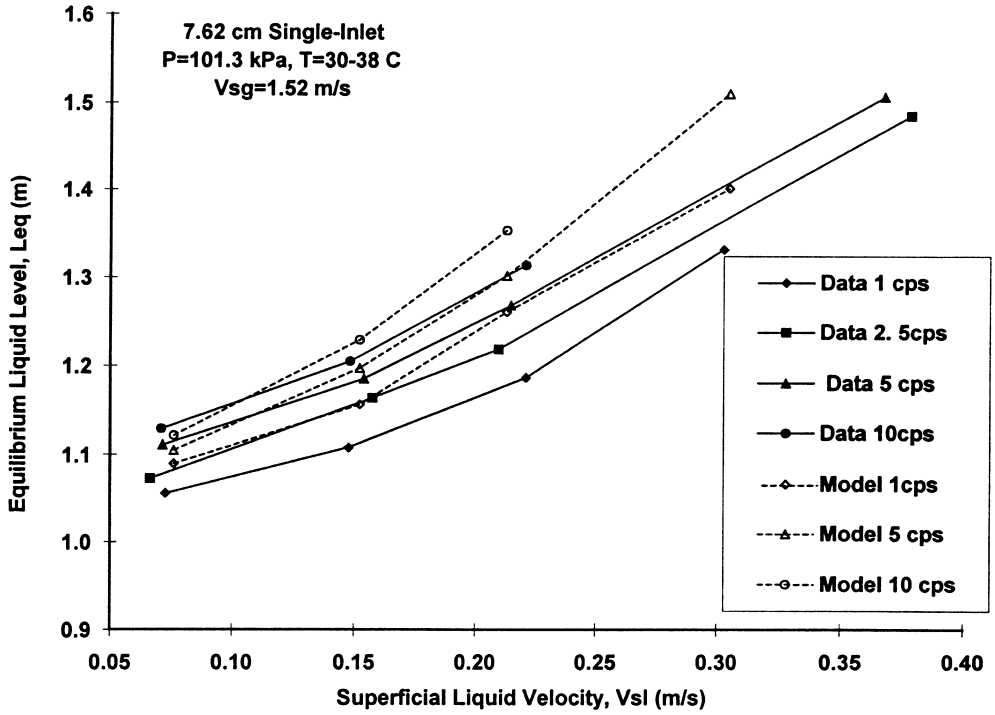

Fig. 5. Comparison of equilibrium liquid level, effect of viscosity ($v_{sg} = 1.52$ m/s).

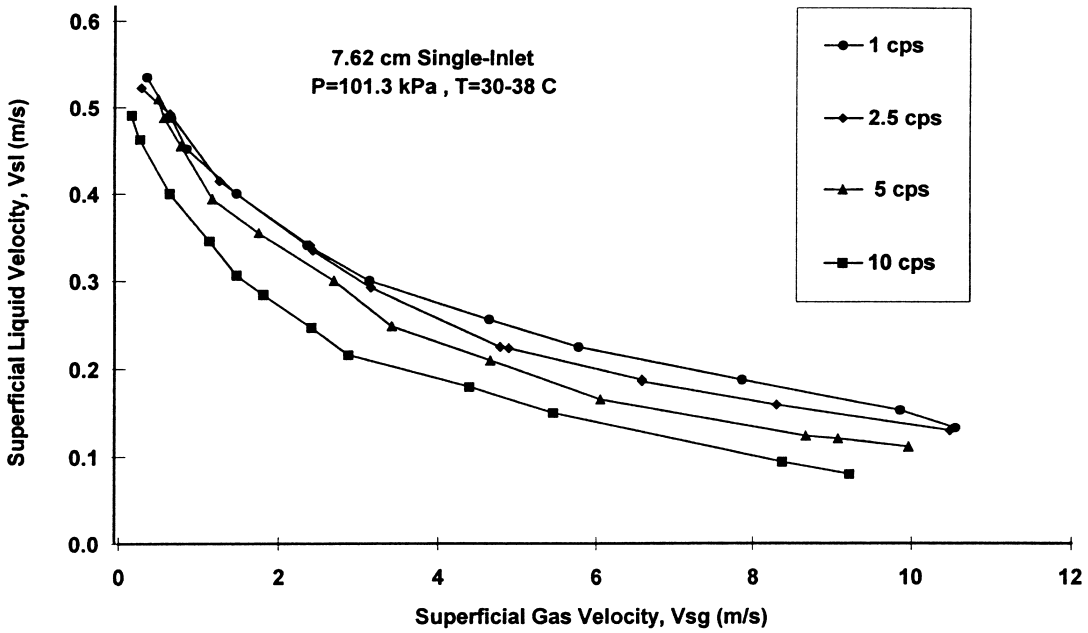

Fig. 6. Effect of viscosity on operational envelope for liquid carry-over.

As shown in Fig. 7, no significant variation of zero-net liquid flow holdup in the upper part of GLCC was observed for the different viscosity runs.

2.3.3.2. Effect of surfactant. The capability of GLCC to handle foam was studied by adding a foam generating surfactant to the water. The objective of this experiment was to investigate whether the GLCC acts as a foam generator or a foam breaker. Two surfactant concentrations were utilized, dropping the surface tension to 47 and 37 dyn/cm. As shown in Fig. 8, foam is generated at low superficial gas velocities and the operational envelope for liquid carry-over is significantly reduced, as compared to the air-water results. However, at high superficial gas velocities, above 6 m/s, due to lower liquid levels below the inlet of the GLCC, foam dissipation is observed. At this condition, the operational envelope is the same as the envelope for the air–water case. This result indicates that GLCC can be used as a foam breaker, if it is operating at high superficial gas velocities and low liquid levels. Absence of significant difference in the operational envelope between the 47 and the 37 dynes/cm case indicates that foaming tendency dictates the flow behavior in the GLCC rather than the surface tension values of the gas–liquid mixture.

2.3.3.3. Effect of operating pressure. As illustrated in Fig. 9, an increase in the GLCC operating pressure results in a marginal reduction of the operational envelope for liquid carry-over for the tested pressure range (Arpandi et al., 1996). This is due to the increased gas density, which increases the drag forces on the liquid phase, enhancing liquid carry-over into the gas stream.

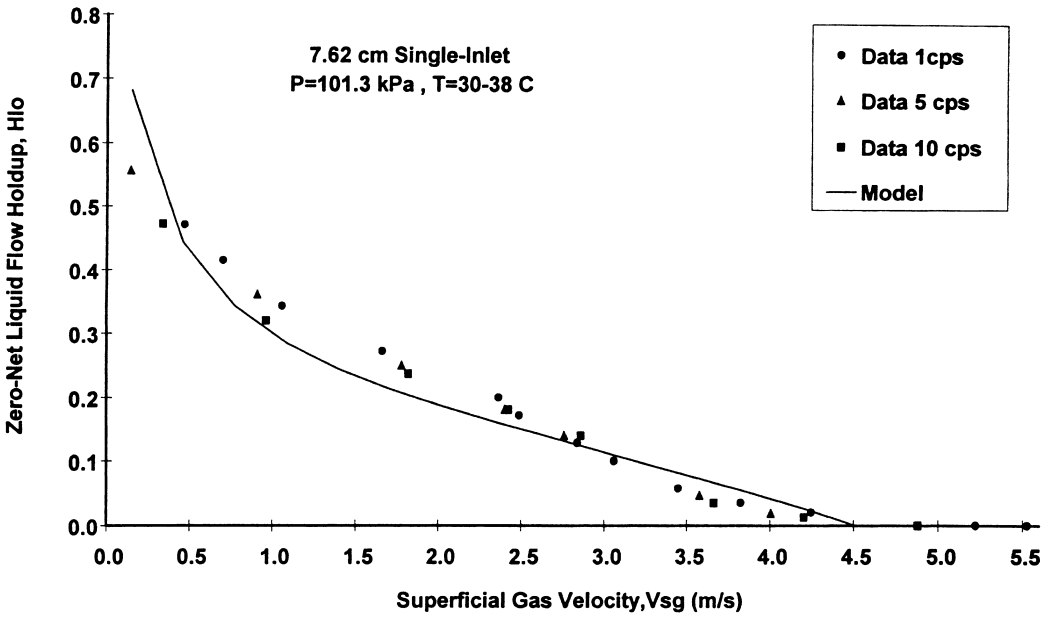

Fig. 7. Comparison of zero-net liquid flow holdup, effect of viscosity.

3. Modeling and results

3.1. Mechanistic modeling

The mechanistic model described below is a modified version of the model presented by Arpandi et al. (1996). The model addresses the following parameters related to the onset of liquid carry-over, namely: equilibrium liquid level, gas–liquid interface, and zero-net liquid flow holdup. The sub-models defining the above parameters are combined for the prediction of the operational envelope for liquid carry-over. The GLCC geometrical parameters and nomenclature for the model are given in Fig. 10. Note that the analysis is carried out for the GLCC in a multiphase flow metering loop configuration.

3.1.1. Equilibrium liquid level

For proper operation of the GLCC, the liquid level must be maintained below the inlet to avoid carrying liquid droplets into the gas leg. Also, the liquid level should be sufficiently high above the liquid exit at the bottom of the GLCC in order to avoid gas carry-under in the liquid stream. Therefore, it is essential to be able to predict the liquid level for proper operation of the GLCC.

The liquid level can be determined by balancing the pressure in the gas and the liquid legs, between the inlet and outlet of the GLCC (P_1 and P_2 in Fig. 10). This model neglects any hydrodynamic interactions between the gas and the liquid phases. Equating the pressure drops

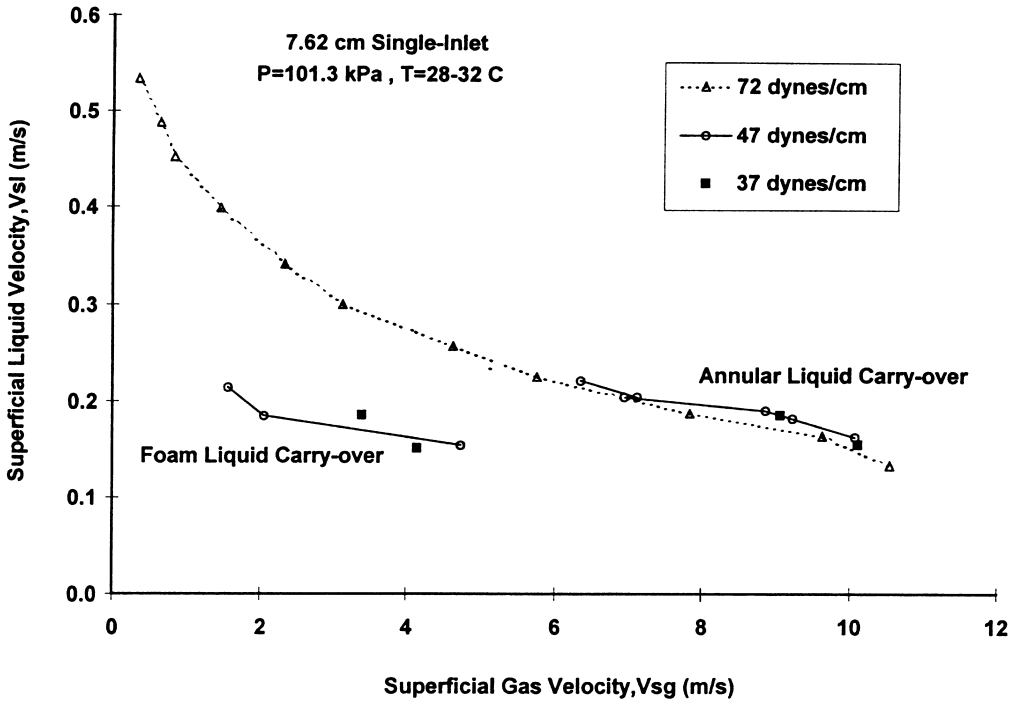

Fig. 8. Effect of surfactants on operational envelope for liquid carry-over.

in the liquid and gas sections, the liquid level can be solved explicitly, as follows:

$$L_{eq} = \frac{\phi_l - \phi_g + \rho_l g L_{l_3} - \rho_g g\left(L_{in} + L_{g_1} - L_{g_3}\right)}{g(\rho_l - \rho_g) - \left(\frac{\rho_l v_{l_1}^2}{2}\frac{f_{l_1}}{D_1}\right)} \tag{1}$$

where Φ_l and Φ_g are the frictional pressure losses in the liquid and gas sections, respectively, and are given by:

$$\phi_l = \frac{\rho_l}{2}\left(\sum_{i=2}^{n}\frac{f_i L_i v_i^2}{D_i} + \sum_{i=1}^{m} K_i v_i^2\right)_l \tag{2}$$

$$\phi_g = \frac{\rho_g}{2}\left(\sum_{i=1}^{p}\frac{f_i L_i v_i^2}{D_i} + \sum_{i=1}^{q} K_i v_i^2\right)_g \tag{3}$$

The first terms in the parentheses of Eqs. (2) and (3) represent the frictional losses in the different pipe segments of the loop, excluding the GLCC section below the inlet, and the second terms represent the losses in the different pipe fittings. Here, n and m represent the

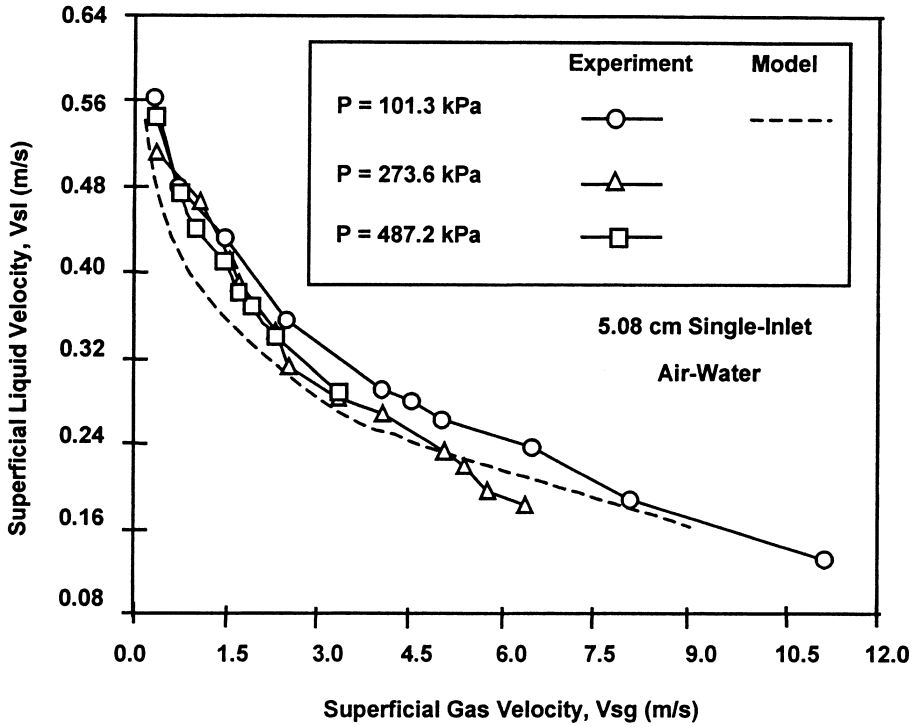

Fig. 9. Effect of pressure on operational for liquid carry-over.

number of pipe segments and pipe fittings, respectively, in the liquid leg, and p and q represent the respective elements in the gas leg.

3.1.2. Gas–liquid interface

The physical model for the determination of the gas–liquid interface shape is given in Fig. 11. The main assumption is that the tangential flow from the inlet into the GLCC generates a forced vortex tangential velocity structure. Millington and Thew (1987) substantiate this assumption.

The model is essentially a pressure balance between points 1 and 4, which results in an equation for the location of the interface at any axial position, z, as a function of the radial coordinate r, namely

$$z(r) = \frac{\Delta P(r)}{g(\rho_l - \rho_g)} \tag{4}$$

where, $\Delta P(r) = \int_r^{R_S} \frac{\rho_m(r)[v_t(r)]^2}{r} dr$ is the pressure difference between points 2 and 3 due to the centrifugal forces. The tangential velocity distribution for a forced vortex (Millington and Thew, 1987) is of the form, $v_t(r) = v_{t_{is}}(\frac{r}{R_s})$, where R_s is the GLCC radius. The inlet slot tangential velocity, $v_{t_{is}}$, can be estimated from the inlet section analysis, as suggested by Gomez (1998). Also, the mixture density surrounding the vortex ρ_m, is assumed to be the liquid density.

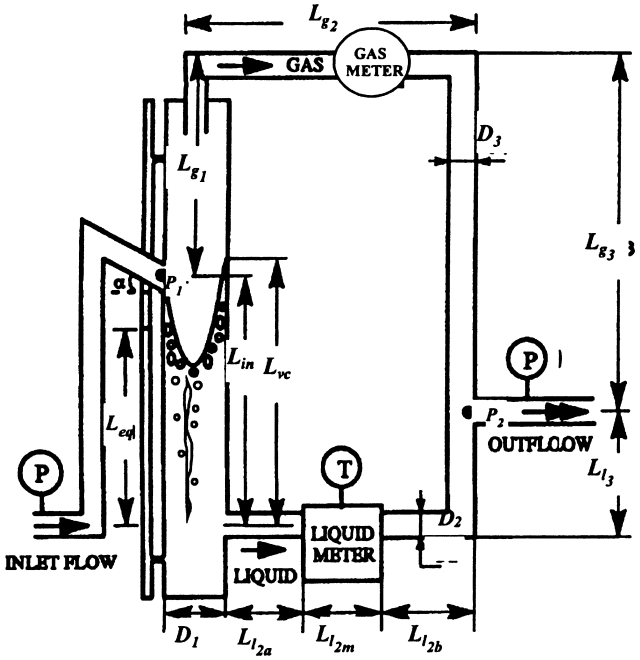

Fig. 10. GLCC nomenclature for the mechanistic model.

The total liquid volume displaced by the gas vortex and gas-core-filament is

$$V_g = \int_{R_c}^{R_s} 2\pi r z(r)\,dr + \frac{\pi}{4} D_c^2 (L_{vc} - L_v) \tag{5}$$

where $L_v = z(R_c)$ and R_c is the gas core-filament radius. The second term in Eq. (5) is the volume of the gas-core-filament that extends from the bottom of the gas core vortex to the liquid exit, as shown in Fig. 11. The height of the liquid, where the gas–liquid interface touches the wall, namely, the vortex crown, is calculated assuming that the total gas volume is submerged in the liquid, as follows:

$$L_{vc} = L_{eq} + \frac{V_g}{A_s} \tag{6}$$

where A_s is the cross sectional area of the GLCC.

3.1.3. Zero-net liquid flow holdup

For zero-net liquid flow conditions, assuming churn/slug flow in the upper part of the GLCC, the gas velocity can be developed from a modified Taylor bubble rise velocity expression, namely

$$v_{g_0} = C_0 v_{sg} + 0.35\sqrt{g D_s \left(\frac{\rho_l - \rho_g}{\rho_l}\right)} \tag{7}$$

where D_s is the GLCC diameter and the flow coefficient for slug/churn flow, C_0, is assumed to be 1.15.

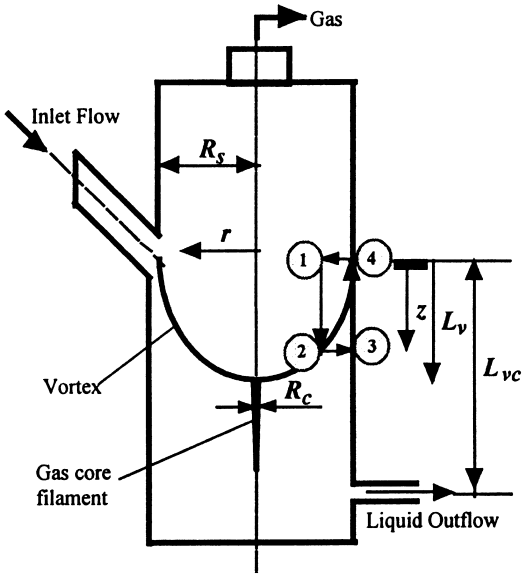

Fig. 11. Gas–liquid interface geometry.

The zero-net liquid flow holdup is given by

$$H_{l_0} = \left[1 - \left(\frac{v_{sg}}{v_{g_0}}\right)\right]\left(1 - \frac{L_d}{L_{g_l}}\right) \tag{8}$$

where L_{g_l} is the total height of the GLCC above the inlet (see Fig. 10). Churn/slug flow occurs only in the lower region, right above the inlet, while at the upper region, liquid is present primarily in the form of droplets. The length of the droplet region, L_d, can be determined from a simplified droplet ballistic analysis. It is equal to the trajectory length of a fine droplet, assuming that the gas void fraction in this region is approximately one. This results in the upward gas velocity being approximately equal to the superficial gas velocity. Thus, the length of the droplet region, L_d, is given by,

$$L_d = \frac{1}{\dfrac{2g_c}{v_{sg}^2} - \dfrac{C_d}{2}(\rho_g v_{sg})^2 \dfrac{3}{32\rho_l \sigma g_c}} \tag{9}$$

Note that Eq. (9) can be rearranged to determine the blowout velocity, v_{b_0}. This is the droplet velocity (v_{sg} in Eq. (9)) for which the length of the droplet region, L_d, is equal to the total height of the GLCC above the inlet. Clearly, for these conditions the zero-net liquid flow holdup, as given by Eq. (8), tends to zero.

The frictional pressure drop in the upper part of the GLCC, above the inlet, is determined by taking into consideration the reduced area of flow of the gas phase due to the presence of liquid. The reduced GLCC diameter is given by $D_{g_0} = D_s\sqrt{1 - H_{l_0}}$ and the increased gas velocity, v_{g_0}, is given by (7). The Reynolds number is therefore given by,

$$Re_{g_0} = \frac{\rho_g v_{g_0} D_{g_0}}{\mu_g}. \tag{10}$$

The interface roughness is assumed to be the same as an equivalent annular film thickness, δ, resulting in a friction factor of the form

$$f_{g_0} = f_{g_0}\left(Re_{g_0}, \frac{\delta}{D_{g_0}}\right) \tag{11}$$

where the equivalent film thickness is given by, $\delta = \frac{D_s - D_{g_0}}{2}$.

3.1.4. Operational envelope for liquid carry-over

Combining the above sub-models enables the prediction of the operational envelope for liquid carry-over. For a given superficial gas velocity, v_{sg}, the superficial liquid velocity, v_{sl}, is determined by a trial and error procedure, equating the pressure drop in the liquid and gas legs (as done for the determination of the equilibrium liquid level). For this case, however, the gravitational and frictional pressure drops in the upper of the GLCC include the effect of the presence of liquid phase at zero-net liquid flow conditions, as follows:

$$\Delta P_{g_l} = -\frac{f_{g_0}\rho_g v_{g_0}^2 (L_{g_l} - L_d)}{2D_{g_0}} - \frac{f_g \rho_g v_{sg}^2 L_d}{2D_s} - \rho_{m_0} g (L_{g_l} - L_d) \tag{12}$$

where f_{g_0} is given by Eq. (11) and the mixture density, ρ_{m_0}, is based on the zero-net liquid flow holdup given by Eq. (8).

For low superficial gas velocities (and high superficial liquid velocities) liquid is present in the upper part of the GLCC in the form of zero-net liquid flow. For these conditions where $L_d < L_{g_1}$, $H_{l_0} > 0$, the equilibrium liquid level is located above the inlet, and is given by:

$$L_{eq} = L_{in} + H_{l_0}\left(L_{g_1} - L_d\right), \quad \left(\text{for } L_d < L_{g_1}\right). \tag{13}$$

For the case of high superficial gas velocities (and low superficial liquid velocities), for which conditions $L_d \geq L_{g_1}$ and, $H_{l_0} \approx 0$, the equilibrium liquid level is located below the inlet, and is given by:

$$L_{eq} = L_{in} - \left(L_{in} - L_{l_3}\right)\frac{v_{sg} - v_{b_0}}{v_{ct} - v_{b_0}}, \quad \left(\text{for } L_d \geq L_{g_1}\right), \tag{14}$$

where v_{b_0} is the blowout velocity that can be determined from (9), and v_{ct} is the critical gas velocity required to initiate carry-over in the form of fine droplets (Taitel et al., 1980), given by,

$$v_{ct} = 2.3351\left(\sigma We\frac{\rho_l - \rho_g}{\rho_g^2}\right)^{0.25} \tag{15}$$

where *We* is the Weber number, assigned a value of 8 for fine droplets occurring at the onset of liquid carry-over.

Eqs. (12)–(15) can be used to determine the total pressure drop in the gas leg under zero-net liquid flow conditions. Similarly, the total pressure drop in the liquid leg could also be determined. Convergence on the superficial liquid velocity, v_{sl}, for a given superficial gas velocity, v_{sg}, is obtained by trial and error, equating the pressure drops in the gas and liquid legs. This yields one point on the operational envelope, which can be repeated for different values of superficial gas velocities to obtain the entire operational envelope for liquid carry-over.

3.2. Model comparison and discussion

This section provides a comparison between the model predictions and the experimental data for the equilibrium liquid level, zero-net liquid flow holdup and the operational envelope for liquid carry-over.

3.2.1. Comparison of equilibrium liquid level

The comparison for the equilibrium liquid level results for the 1, 5 and 10 cps liquid viscosity runs are given in Fig. 5 for a superficial gas velocity of 1.52 m/s. The agreement between the model prediction and the data is fairly good. Similar agreement is also obtained for higher superficial gas velocities of 4.57 and 6.10 m/s (Movafaghian, 1997). The error is of the order of 0.06 m for most of the cases, which is less than 5%. Higher errors, around 0.12 m or 10%, occur at high superficial liquid velocities larger than 0.3 m/s.

3.2.2. Comparison of zero-net liquid flow holdup

Comparison of the zero-net liquid flow holdup model with the data is given in Fig. 7. The model cuts through the experimental results indicating very good agreement with the data. Note that the proposed model is independent of liquid viscosity. This is consistent with the data, which show only slight variation with the liquid viscosity.

3.2.3. Comparison of operational envelope for liquid carry-over

The ultimate goal of the model is the prediction of the operational envelope for liquid carry-over. Figs. 12 and 13 show the comparison of the operational envelope for liquid carry-over for the 1 and 10 cps liquid viscosity cases, respectively. The figures show the comparison of the operational envelope for liquid carry-over (lower curves, left-hand side y-axis) and also comparison of the equilibrium liquid level at the operational envelope conditions (upper curves, right-hand side y-axis). Very good agreement is observed between the model predictions and the experimental data. The model seems to capture the physics of the flow as it tracks the decrease in the operational envelope for liquid carry-over with increasing liquid viscosity. Movafaghian (1997) may be referred for similar results corresponding to 2.5 and 5 cps liquid viscosity cases.

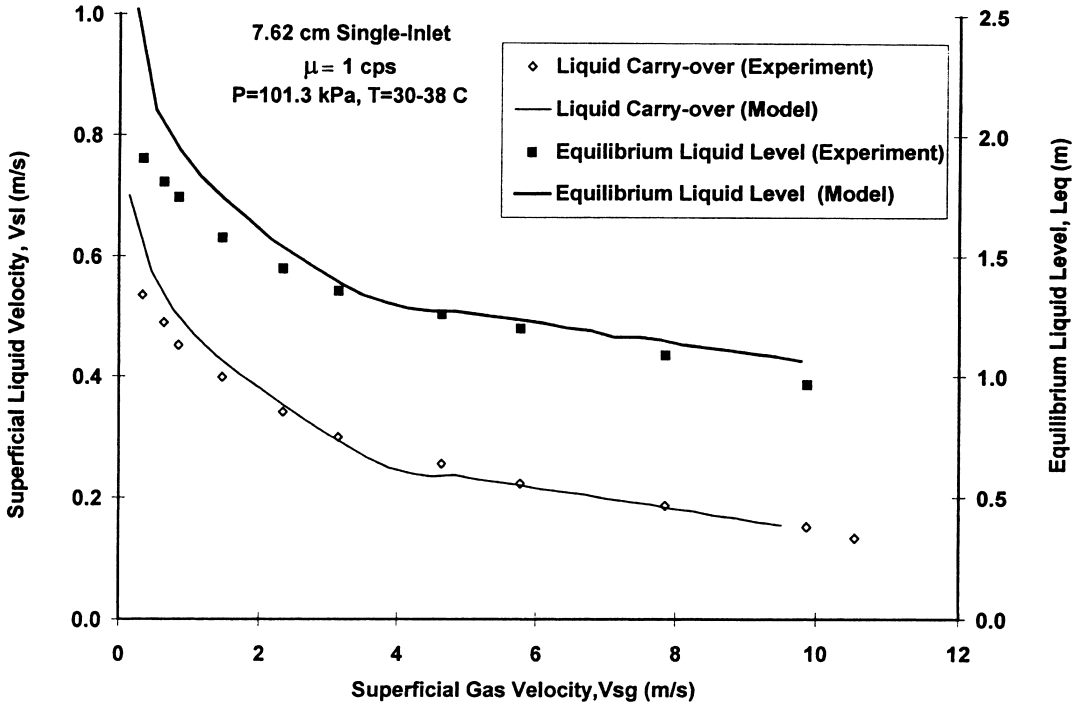

Fig. 12. Comparison of operational envelope for liquid carry-over, effect of viscosity (1 cps).

4. Summary and conclusions

The effects of geometry, fluid physical properties and pressure on the hydrodynamics of two-phase flow in GLCC compact separators have been studied theoretically and experimentally. Several sets of experimental data were collected for single and dual inlet configurations, three recombination points of the gas and the liquid legs, various system pressures, liquid viscosities and concentrations of foam generating surfactant. The acquired data include the operational envelope for liquid carry-over, equilibrium liquid level and zero-net liquid flow holdup.

Comparison of the operational envelopes for liquid carry-over reveals that the dual-inlet configuration is superior to the single-inlet, for superficial gas velocities below 7 m/s due to the pre-separation occurring in the dual-inlet. Examination of the liquid carry-over operational envelope data for the different liquid viscosities shows a consistent and continuous reduction of the operational envelope region with increase in viscosity. Also, the equilibrium liquid level increases as viscosity increases due to the increased frictional losses in the liquid leg. With surfactant additives, foam is generated at low superficial velocities, reducing significantly the operational envelope for liquid carry-over, as compared to the air–water results. However, for high superficial velocities, above 6 m/s, due to lower liquid levels in the GLCC and more efficient separation, the operational envelopes are the same as that of the air–water case. Increasing the pressure resulted in a marginal reduction of the operational envelope for liquid carry-over for the tested pressure range.

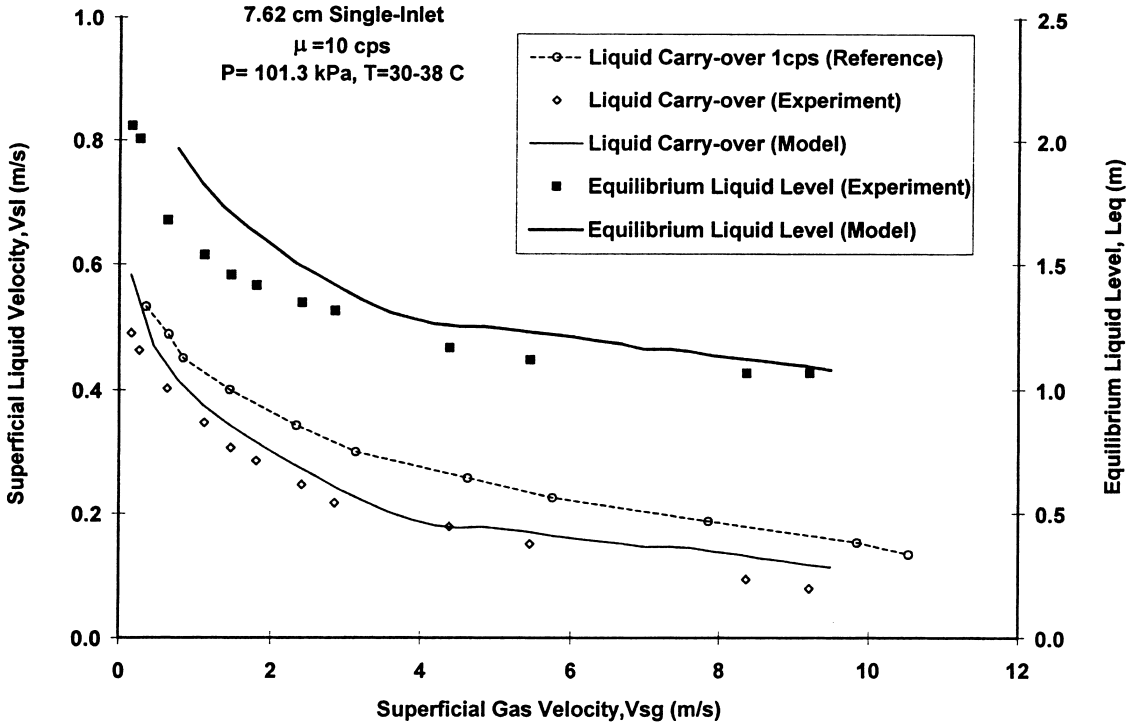

Fig. 13. Comparison of operational envelope for liquid carry-over, effect of viscosity (10 cps).

Comparison between the modified Arpandi et al. (1996) mechanistic model predictions and the experimental data shows very good agreement with respect to the equilibrium liquid level, zero-net liquid flow holdup and the operational envelope for liquid carry-over.

Acknowledgements

The authors wish to thank Chevron Petroleum Technology Co. and all the other member companies of the Tulsa University Separation Technology Projects (TUSTP) for supporting this investigation.

References

Arato, E.G., Barnes, N.D. 1992. In-line free vortex separator used for gas/liquid separation within a novel two-phase pumping system. In: Svarovsky, L., Thew, M.T., Brookfield, V.T. (Eds.), Hydrocyclones-Analysis and Application. Kluwer Academic Publishers, Dordrecht, pp. 377–396.

Arpandi I.A., Joshi A.R., Shoham, O., Shirazi, S., Kouba, G.E., Hydrodynamics of two-phase flow in gas–liquid cylindrical cyclone separators. SPE 30683, Presented at SPE 70th Annual Meeting, Dallas, October 22–26, 1995, SPEJ, December 1996, pp. 427–436.

Baker, A.C., Entress, J.H., 1992. VASPS (Vertical Annular Separation Pumping System) Subsea separation and pumping system, Trans. I. Chem. E. 70 (Part A), 9–16. Paper presented at the Institution of Chemical Engineers Conference, Subsea Separation and Transport III, London, May 23–24, 1991.

Bandyopadhyay, P.R., Pacifico, G.C., Gad-el-Hak, M., 1994. Sensitivity of a gas-core vortex in a cyclone-type gas–liquid separator, Advanced Technology and Prototyping Division, Naval Undersea Warfare Center Division, Newport, Rhode Island.

Cowie, D. Vertical caisson slugcatcher performance, presented at the Institution of Chemical Engineers Conference, Subsea Separation and Transport III, London, May 23–24, 1991. Trans. IChemE. 70, part A, January 1992, 25–31.

Davies, E.E, Watson, P., 1979. Miniaturized separators for offshore platforms. In: Proceedings of the 1st New Technology for Exploration and Exploitation of Oil and Gas Reserves Symposium, Luxembourg, April, 75–85.

Erdal, F.M., 1996. CFD simulation of single-phase and two-phase flow in gas–liquid cylindrical cyclone separator. M.S. thesis, The University of Tulsa.

Erdal, F.M., Shirazi, S.A., Shoham, O., Kouba, G.E. CFD simulation of single-phase and two-phase flow in gas–liquid cylindrical cyclone separators. SPE 36645, presented at the SPE 71st Annual Meeting, Denver, CO, October 6–9, 1996.

Forsyth, R.A., 1984. Cyclone separation in natural gas transmission systems — the design and performance of cyclones to take debris out of natural gas. Chemical Engineer, London, pp. 37–41.

Gomez, L.E., 1998. A state-of-the-art simulator and field application design of gas–liquid cylindrical cyclone separators. M.S. thesis, The University of Tulsa.

Kanyua, J.F., Freeston, D.H., 1985. Vertical flow centrifugal separator — effects of geometry. Trans. of the Geothermal Resources Council, New Zealand 9 (11), 251–256.

Kouba, G.E., Shoham, O., 1996. A review of gas–liquid cylindrical cyclone (GLCC) technology, presented at the. In: Production Separation Systems, International Conference, Aberdeen, England, April 23-24.

Kouba, G.E, Shoham, O., Shirazi, S., 1995. Design and performance of gas–liquid cylindrical cyclone separators. In: Proceedings of the BHR Group 7th International Meeting on Multiphase Flow, Cannes, France, June 7–9, 307–327.

Kurokawa, J., Ohtaik, T., 1995. Gas–liquid flow characteristics and gas-separation efficiency in a cyclone separator. Gas Liquid Flows ASME FED-225, 51–57.

Marti, S., Erdal, F., Shoham, O., Shirazi, S., Kouba, G. Analysis of gas carry-under in gas–liquid cylindrical cyclones, Presented at the Hydrocyclones 1996 International Meeting. St. John College, Cambridge, England, April 2–4, 1996.

Millington, B.C., Thew, M.T., 1987. LDA study of component velocities in air–water models of steam–water cyclone separators. In: Proceeding of the 3rd International Conference on Multiphase Flow, The Hague, The Netherlands, May 18, 115–125.

Motta, B.R.F., Erdal, F.M., Shirazi, S.A., Shoham, O., Rhyne, L.D., 1997. Simulation of single-phase and two-phase flow in gas–liquid cylindrical cyclone separators. In: Proceedings ASME Summer Meeting, FEDSM97-3554, Vancouver, Canada, June 22–26.

Movafaghian, S., 1997. The effects of geometry, fluid properties and pressure on the flow hydrodynamics in GLCC separators. M.S. thesis, The University of Tulsa.

Nebrensky, N.T., Morgan, G.E., Oswald, B.J., 1980. Cyclone for gas/oil separation. In: Proceedings of the International Conference on Hydrocyclones, Churchill College, Cambridge, UK, 1980, paper No.12, 167–177.

Oranje, I.L., 1990. Cyclone-type separators score high in comparative tests. Oil and Gas Journal 88 (4), 54–57.

Reydon, R.F., Gauvin, W.H., 1981. Theoretical and experimental studies of confined vortex flow. The Canadian Journal of Chemical Engineering 59, 14–23.

Taitel, Y., Barnea, D., Dukler, A.E., 1980. Modeling flow pattern transition for steady upward gas–liquid flow in vertical tubes. AIChE J 26 (3), 345–351.

Weingarten, J.S., Kolpak, M.M., Mattison, S.A., Williamson, M.J. New design for compact liquid–gas partial separation: downhole and surface installations for artificial lift applications. SPE 30637, Presented at the SPE 70th Annual Meeting, Dallas, October 22–25, 1995.

Wolbert, D., Ma, B.F., Aurelle, Y., Seureau, J., 1995. Efficiency estimation of liquid–liquid hydrocyclones using trajectory analysis. AIChE J 41 (6), 1395–1402.

Zhikarev, A.S., Kutepov, A.M., Solov'ev, V., 1985. Design of a cyclone separator for the separation of gas–liquid mixtures. Chemical and Petroleum Engineering 21 (4), 196–198 (Translated from Russian).